PROCEEDINGS OF SCIENCE

Transverse momentum-dependent parton distributions for longitudinally polarized nucleons from domain wall fermion calculations at the physical pion mass

M. Engelhardt,[a,*] **N. Hasan,**[b] **T. Izubuchi,**[c] **C. Kallidonis,**[d] **S. Krieg,**[e,f,g] **S. Meinel,**[h] **J. Negele,**[i] **A. Pochinsky,**[i] **G. Silvi**[b,j] **and S. Syritsyn**[k]

[a] *Department of Physics, New Mexico State University, Las Cruces, NM 88003, USA*
[b] *Bergische Universität Wuppertal, 42119 Wuppertal, Germany*
[c] *Physics Department, Brookhaven National Laboratory, Upton, NY 11973, USA*
[d] *Thomas Jefferson National Accelerator Facility, Newport News, VA 23606, USA*
[e] *JARA & IAS, Jülich Supercomputing Centre, Forschungszentrum Jülich, 52425 Jülich, Germany*
[f] *Helmholtz-Institut für Strahlen- und Kernphysik, Universität Bonn, 53115 Bonn, Germany*
[g] *Center for Advanced Simulation and Analytics (CASA), Forschungszentrum Jülich, 52425 Jülich, Germany*
[h] *Department of Physics, University of Arizona, Tucson, AZ 85721, USA*
[i] *Center for Theoretical Physics, Massachusetts Institute of Technology, Cambridge, MA 02139, USA*
[j] *Jülich Supercomputing Centre, Forschungszentrum Jülich, 52425 Jülich, Germany*
[k] *Department of Physics and Astronomy, Stony Brook University, Stony Brook, NY 11794, USA*

E-mail: engel@nmsu.edu

Previous Lattice QCD calculations of nucleon transverse momentum-dependent parton distributions (TMDs) focused on the case of transversely polarized nucleons, and thus did not encompass two leading-twist TMDs associated with longitudinal polarization, namely, the helicity TMD and the worm-gear TMD corresponding to transversely polarized quarks in a longitudinally polarized nucleon. Based on a definition of TMDs via hadronic matrix elements of quark bilocal operators containing staple-shaped gauge connections, TMD observables characterizing the aforementioned two TMDs are evaluated, utilizing an RBC/UKQCD domain wall fermion ensemble at the physical pion mass.

The 39th International Symposium on Lattice Field Theory (Lattice2022),
8-13 August, 2022
Bonn, Germany

*Speaker

PoS(LATTICE2022)103

1. Introduction

Transverse momentum-dependent parton distribution functions [1] (TMDs) embody fundamental information on the three-dimensional partonic structure of hadrons. Complementary to generalized parton distributions (GPDs), which provide insight into the transverse spatial structure through their Fourier transforms, impact parameter-dependent parton distributions, TMDs encode the distribution of transverse momentum among the partons. From the point of view of a Lorentz frame in which a nucleon of mass m_N is propagating in the 3-direction with a large momentum, $P^+ \equiv (P^0 + P^3)/\sqrt{2} \gg m_N$, the minus component of the quark momentum k becomes ignorable, $k^- \equiv (k^0 - k^3)/\sqrt{2} \ll m_N$, as a consequence of which TMDs principally depend on the parton longitudinal momentum fraction $x = k^+/P^+$ and the parton transverse momentum vector k_T. Generic TMDs $f(x, k_T)$ are regarded as being integrated over the k^- component.

The hadronic structure encoded in TMDs inherently influences angular asymmetries observed in experimental processes such as semi-inclusive deep inelastic scattering (SIDIS) and the Drell-Yan (DY) process. Motivated by past observations at COMPASS, HERMES and JLab [2–4], current and upcoming experimental efforts within the JLab 12 GeV program and the planned electron-ion collider (EIC) place a strong emphasis on the further investigation of TMDs. Central to the analysis of the experimental signatures and the connection to the underlying hadronic structure distilled into the TMDs is a factorization framework. A prominent such framework is the one developed in [5–8], which is simultaneously well suited to connect the QCD definition of TMDs to Lattice QCD calculations, as will be laid out in more detail below. A feature of TMD factorization that has attracted considerable interest, and that illustrates its enhanced complexity compared to standard collinear factorization, is the process dependence of TMDs introduced by initial or final state interactions between the active quark parton and the hadron remnant. In particular, the relative sign change of the Sivers TMD $f_{1T}^{\perp}$, as extracted from SIDIS vs. DY in transversely polarized nucleons, has received intense scrutiny [9–11].

Not least as a consequence of the focus on this effect and others observed in transversely polarized nucleons, also past lattice TMD calculations [12–14] have concentrated on the case of transverse nucleon polarization. This has left the longitudinally polarized sector largely unexplored, with the notable exception of generalized TMD (GTMD) investigations of quark orbital angular momentum in the nucleon [15–17]. The present study closes this gap; all leading-twist quark TMD observables have thereby now been explored within the lattice TMD program previously developed in [12–14].

2. Construction of TMD observables

A construction of TMD ratio observables that to a large extent avoids the complications that arise in the definition of isolated TMDs [18–20], and is consequently comparatively straightforward to implement within Lattice QCD, is described in detail in [12]. To summarize, TMDs are defined based on the fundamental nonlocal correlator

$$\widetilde{\Phi}^{[\Gamma]}_{\text{unsubtr.}}(b, P, S, \ldots) \equiv \frac{1}{2}\langle P, S|\, \bar{q}(0)\, \Gamma\, \mathcal{U}[0, \eta v, \eta v + b, b]\, q(b)\, |P, S\rangle \tag{1}$$

evaluated in a hadron state with momentum P and spin S. The quark operator separation b is Fourier conjugate to the quark momentum k. Γ denotes an arbitrary Dirac γ-matrix structure,

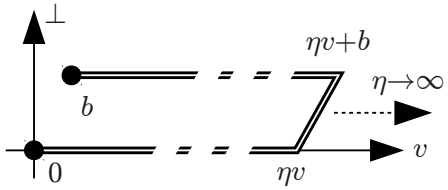

Figure 1: Path of the Wilson line $\mathcal{U}$ in the matrix element (1).

and the quark operators are connected by a staple-shaped Wilson line $\mathcal{U}$ composed of straight-line segments running between the positions specified in its argument, as also illustrated in Fig. 1. The direction of the staple legs is given by the unit vector v, whereas their length is parametrized by η (below, both positive and negative values of η will be allowed in order to encode a reversal of direction of the staple legs in a simple manner). An important complication in the definition of TMDs arises owing to the divergences associated with $\mathcal{U}$, which must be compensated by a "soft factor". This soft factor is multiplicative and can thus be cancelled, along with additional wave function renormalization factors associated with the quark operators, by forming appropriate TMD ratios. This is the scheme pursued in the following, as a result of which specific consideration of the soft factor is avoided.

Furthermore, the most naive choice of v as a light-cone vector introduces rapidity divergences, which in the scheme advanced in [5–7] are regulated by taking v off the light cone into the space-like region, the approach to the light cone being governed by perturbative evolution equations. In the following, the Collins-Soper type evolution parameter measuring the deviation of v from the light cone will be chosen as

$$\hat{\zeta} = \frac{v \cdot P}{|v|\,|P|} \,. \tag{2}$$

The light-cone limit corresponds to $\hat{\zeta} \to \infty$. This prescription of employing space-like v renders the connection to Lattice QCD particularly straightforward, as detailed below.

A crucial further element of the present treatment is the decomposition of the correlator $\widetilde{\Phi}^{[\Gamma]}_{\text{unsubtr.}}$ defined in (1) into Lorentz-invariant amplitudes, denoted below by $\widetilde{A}_{iB}$. This decomposition will allow for a simple translation of results between the Lorentz frame in which TMDs are defined, as discussed up to this point, and the Lorentz frame suited for a Lattice QCD calculation, introduced further below. At leading twist, the decomposition for nucleons reads [12]

$$\begin{aligned}
\frac{1}{2P^+}\widetilde{\Phi}^{[\gamma^+]}_{\text{unsubtr.}} &= \widetilde{A}_{2B} + im_N\epsilon_{ij}b_iS_j\widetilde{A}_{12B} \\
\frac{1}{2P^+}\widetilde{\Phi}^{[\gamma^+\gamma^5]}_{\text{unsubtr.}} &= -\Lambda\widetilde{A}_{6B} + i[(b\cdot P)\Lambda - m_N(b_T\cdot S_T)]\widetilde{A}_{7B} \\
\frac{1}{2P^+}\widetilde{\Phi}^{[i\sigma^{i+}\gamma^5]}_{\text{unsubtr.}} &= im_N\epsilon_{ij}b_j\widetilde{A}_{4B} - S_i\widetilde{A}_{9B} - im_N\Lambda b_i\widetilde{A}_{10B} + m_N[(b\cdot P)\Lambda - m_N(b_T\cdot S_T)]b_i\widetilde{A}_{11B} \,,
\end{aligned} \tag{3}$$

where Λ denotes the nucleon helicity (i.e., $S^+ = \Lambda P^+/m_N$, $S^- = -\Lambda m_N/2P^+$). Specializing to the case of longitudinal polarization, $S_T = 0$, and focusing on momentum fraction x-integrated TMDs, accessed in b-space by considering $b\cdot P = 0$, the amplitudes $\widetilde{A}_{2B}$, $\widetilde{A}_{6B}$ and $\widetilde{A}_{10B}$ can be

readily isolated[1] and serve to define the following TMD ratio observables in which multiplicative soft factors associated with the Wilson line $\mathcal{U}$ and wave function renormalization factors attached to the quark operators in (1) at finite separation b are cancelled:

- The generalized $h_{1L}^{\perp}$ worm-gear shift

$$\langle k_x \rangle_{LT}(b_T^2, \ldots) = -m_N \widetilde{A}_{10B}(-b_T^2, \ldots)/\widetilde{A}_{2B}(-b_T^2, \ldots) = m_N \tilde{h}_{1L}^{\perp[1](1)}(b_T^2, \ldots)/\tilde{f}_1^{[1](0)}(b_T^2, \ldots) \tag{4}$$

  where the expression on the right-hand side establishes the connection to Fourier-transformed TMD moments, cf. [12]. In the formal $b_T \to 0$ limit, (4) represents the average transverse momentum k_x of quarks polarized in the same transverse ("T") direction, i.e., here, the x-direction, in a longitudinally ("L") polarized nucleon, normalized to the number of valence quarks. It should be noted that the $b_T^2 = 0$ limit introduces additional divergences that require adequate treatment compared to the ("generalized") finite b_T case.

- The generalized axial charge

$$\Delta\Sigma(b_T^2, \ldots) = -\widetilde{A}_{6B}(b_T^2, \ldots)/\widetilde{A}_{2B}(b_T^2, \ldots) = \tilde{g}_1^{[1](0)}(b_T^2, \ldots)/\tilde{f}_1^{[1](0)}(b_T^2, \ldots) \tag{5}$$

  which, in the $b_T \to 0$ limit, reduces to the standard axial charge, normalized to the number of valence quarks. In this case, the additional divergences in the $b_T^2 = 0$ limit are associated with the standard renormalization factors Z_A and Z_V in the numerator and denominator, respectively; using domain wall fermions, as is done in the following lattice calculation, one has $Z_A = Z_V$ and these renormalization factors cancel[2].

3. Lattice calculation

In a Lattice QCD calculation, the operator of which one is taking a hadronic matrix element in (1) has to be located at one single Euclidean insertion time. On the other hand, the operator as defined above in general extends into the (Minkowski) temporal direction. However, since all separations in the operator, controlled by the four-vectors b and v, are space-like, the problem can be boosted to a Lorentz frame in which the entire operator indeed exists at a single time, and the lattice calculation can be performed in that frame. This is the point where a formulation employing a space-like direction v for the purpose of regulating rapidity divergences is crucial. Furthermore, having decomposed the resulting $\widetilde{\Phi}^{[\Gamma]}_{\text{unsubtr.}}$ into the invariant amplitudes $\widetilde{A}_{iB}$, the results for those amplitudes are immediately also applicable in the Lorentz frame in which (1) was originally defined; TMD observables of the type (4) and (5) are thus determined.

The data obtained in a lattice calculation are necessarily limited to a finite staple length η and a finite rapidity parameter $\hat{\zeta}$, and they must be extrapolated to the limits $\eta \to \infty$ and $\hat{\zeta} \to \infty$. As will

[1] The amplitude $\widetilde{A}_{4B}$ associated with the Boer-Mulders effect, observed in unpolarized hadrons, will not be considered further here, since it has already been discussed in previous studies focusing on transversely polarized or unpolarized hadrons [12–14].

[2] Preserving chiral symmetry in the fermion discretization moreover prevents the appearance of operator mixing effects [21–24] induced by the breaking of chiral symmetry. Such effects would invalidate the cancellation of renormalization factors through taking ratios such as (4) and (5), since they would generate additional additive terms in the numerators and denominators.

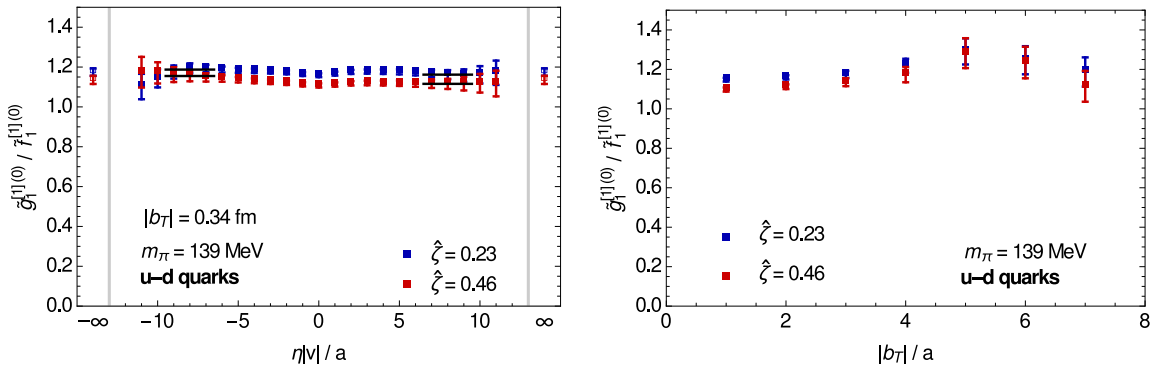

Figure 2: Isovector generalized axial charge in the nucleon. Left: Dependence on the staple length η for fixed $|b_T|$ and two values of $\hat{\zeta}$; the extrapolation to the $|\eta| \to \infty$ SIDIS/DY limit is described in the main text. Right: SIDIS/DY limit as a function of $|b_T|$ for two values of $\hat{\zeta}$. Error bars show statistical uncertainties only.

be seen below, the former extrapolation can be controlled for a substantial range of the parameter space employed in this work. The latter extrapolation is more challenging, since large $\hat{\zeta}$ can only be achieved using large hadron momentum P, and the set of P that can be accessed reliably in a lattice calculation is fairly limited. In the present study, no quantitative extrapolation will be attempted, but data will be presented for two values of $\hat{\zeta}$ that suggest that the variation with $\hat{\zeta}$ is mild. Quantitative extrapolations were presented in the dedicated study [13] of the Boer-Mulders effect in the pion.

The present investigation utilized a 2+1 flavor domain wall fermion ensemble provided by the RBC/UKQCD Collaboration, on a $48^3 \times 96$ lattice with spacing $a = 0.114\,\text{fm}$, with pion mass close to the physical limit, $m_\pi = 139\,\text{MeV}$ [25]. On the 130 gauge configurations in the ensemble, an all-mode averaging scheme [26] was implemented, evaluating 33280 low-accuracy and 520 exact samples for bias correction. A significant source of systematic bias, evident in some of the results discussed below, is the rather small source-sink separation $8a = 0.91\,\text{fm}$ that was employed in this exploratory calculation to control statistical fluctuations. Two nucleon momenta, $P_3 = 2\pi/L$ and $P_3 = 4\pi/L$ (where $L = 48a$ denotes the spatial extent of the lattice), were used, corresponding to $\hat{\zeta} = 0.23$ and $\hat{\zeta} = 0.46$.

Fig. 2 shows results for the isovector generalized axial charge in the nucleon. In the isovector, $u - d$ quark combination, diagrams in which the operator is inserted into a disconnected quark loop cancel; such diagrams were not evaluated in this study. The left-hand panel displays the dependence on the staple length η for a fixed operator separation $|b_T|$; data for two values of $\hat{\zeta}$ are shown. Evidently, the η-dependences of the moments of the unpolarized and helicity TMDs f_1 and g_1 closely track one another, leading to virtually constant behavior of the ratio. Extrapolation to $|\eta| \to \infty$ is achieved by the plateau fits indicated by the horizontal lines, which are averaged over the plateaus at positive and negative η in view of the T-even nature of the observable. $\eta \to \infty$ corresponds to the SIDIS limit, whereas $\eta \to -\infty$ corresponds to the DY limit. The data at the two values of $\hat{\zeta}$ do not differ to a statistically significant extent, suggesting a merely mild dependence on $\hat{\zeta}$. The right-hand panel summarizes the $|\eta| \to \infty$ SIDIS/DY limits as a function of $|b_T|$. Also the dependence on $|b_T|$ is mild and not distinguishable from a constant to statistically significant degree.

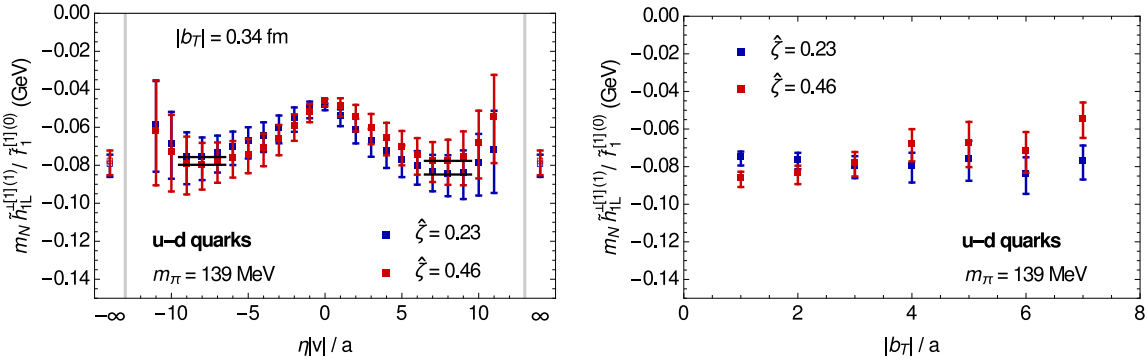

Figure 3: Isovector generalized $h_{1L}^{\perp}$ worm-gear shift in the nucleon. Left: Dependence on the staple length η for fixed $|b_T|$ and two values of $\hat{\zeta}$; the extrapolation to the $|\eta| \to \infty$ SIDIS/DY limit is described in the main text. Right: SIDIS/DY limit as a function of $|b_T|$ for two values of $\hat{\zeta}$. Error bars show statistical uncertainties only.

However, the magnitude of the generalized axial charge obtained here betrays a systematic bias that is presumably owed to excited state contaminations resulting from the small source-sink separation used in the calculation. The data suggest a $b_T = 0$ limit significantly below the experimental value $\Delta\Sigma(b_T = 0) = 1.272$. Such deficits have been widely reported and analyzed in the literature [27–29] and thus their appearance in the present calculation does not come as a surprise. Considerable, dedicated efforts are ultimately required to resolve these discrepancies (see, e.g., [29]).

Fig. 3 shows results for the isovector generalized $h_{1L}^{\perp}$ worm-gear shift in the nucleon. The left-hand panel displays the dependence on the staple length η for a fixed operator separation $|b_T|$; data for two values of $\hat{\zeta}$ are shown. In this observable, appreciable final/initial state interaction effects are seen as one increases $|\eta|$ to approach the SIDIS/DY limits. This worm-gear shift is again a T-even observable, and the extrapolation $|\eta| \to \infty$ is obtained by averaging over the plateau fits indicated by the horizontal lines. As with the generalized axial charge, the data for the two values of $\hat{\zeta}$ do not differ significantly, suggesting a mild dependence on $\hat{\zeta}$. The right-hand panel summarizes the results for the $|\eta| \to \infty$ SIDIS/DY limit as a function of $|b_T|$. Again, the dependence on $|b_T|$ is mild. The blue $\hat{\zeta} = 0.23$ data are not distinguishable from a constant within the statistical uncertainties and the red $\hat{\zeta} = 0.46$ data exhibit at most a weak trend as $|b_T|$ is varied. Interesting, however, is the magnitude of the result: A very robust feature of a wide variety of quark models that differ from one another qualitatively in many other respects is that the $h_{1L}^{\perp}$ and g_{1T} worm-gear TMDs are predicted to have the same magnitude (and opposite sign). This includes the spectator model [30], the light-front constituent quark model [31], the bag model [32], the light-front quark-diquark model [33], the light-front version of the chiral quark-soliton model [34], and the covariant parton model [35], in which also the nonrelativistic limit can be consistently formulated. On the other hand, Fig. 4 displays results for the g_{1T} worm-gear shift obtained in a transversely polarized nucleon in a lattice calculation on the same ensemble with the same computational methodology (including the source-sink separation $8a = 0.91$ fm). Comparing with the right-hand panel in Fig. 3, the $h_{1L}^{\perp}$ and g_{1T} worm-gear shifts do have opposite sign, but the obtained magnitudes differ significantly, by close to a factor 2. Even though, as has been emphasized above, the present computational

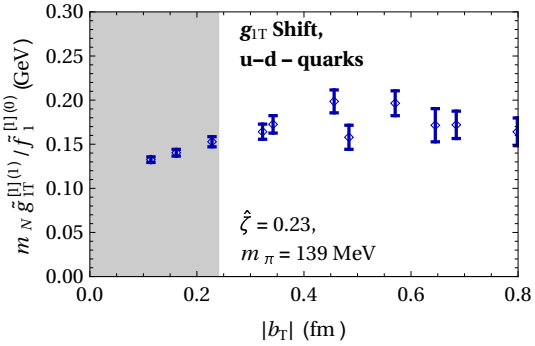

Figure 4: Isovector generalized g_{1T} worm-gear shift in the nucleon in the SIDIS/DY limit as a function of $|b_T|$ for $\hat{\zeta} = 0.23$, to be contrasted with Fig. 3 (right). Data in the shaded region at small $|b_T|$ may be affected by significant finite lattice spacing effects. Error bars show statistical uncertainties only.

setup is still beset by significant systematic uncertainties, the discrepancy between the magnitudes of the $h_{1L}^\perp$ and g_{1T} worm-gear shifts seen in Figs. 3 and 4 appears sufficiently marked as to make an explanation purely through systematic biases in the calculational scheme seem unlikely. The discrepancy rather appears more likely to be a manifestation of strong gluonic dynamical effects present in full QCD that are not captured by quark models.

4. Summary

As part of an ongoing program exploring TMD observables within Lattice QCD, the present investigation focused on longitudinally polarized nucleons. Results were obtained for the generalized axial charge (5) and the generalized $h_{1L}^\perp$ worm-gear shift (4), which had hitherto not been studied; all leading-twist quark TMD observables have thereby now been explored within the lattice TMD program. The data were generated using a RBC/UKQCD domain wall fermion ensemble at the pion mass $m_\pi = 139\,\mathrm{MeV}$. To mitigate statistical fluctuations, a fairly small source-sink separation 0.91 fm was employed in this exploratory calculation, leading to appreciable excited state contaminations that are manifested in the magnitude of the extracted generalized axial charge. The most striking outcome of this study is the magnitude found for the generalized $h_{1L}^\perp$ worm-gear shift, which differs by close to a factor 2 from its counterpart, the g_{1T} worm-gear shift associated with longitudinally polarized quarks in a transversely polarized nucleon. In a wide range of quark models, these two worm-gear shifts are predicted to have the same magnitude (and opposite sign, as is indeed found within the present investigation). Despite the significant systematic biases still contained in the calculational scheme employed, a discrepancy this marked appears likely to reflect genuine physical effects generated by the gluonic dynamics in the nucleon that are not captured by quark models. Additional studies comparing the two worm-gear shifts with reduced systematic uncertainties are necessary to draw more definite conclusions regarding this interpretation.

Acknowledgments

Computing time granted by the John von Neumann Institute for Computing (NIC) and provided on the supercomputer JURECA [36] (Booster module) at Jülich Supercomputing Centre (JSC) is gratefully acknowledged, as are resources provided by the U.S. DOE Office of Science through the National Energy Research Scientific Computing Center (NERSC), a DOE Office of Science User Facility, under Contract No. DE-AC02-05CH11231. Calculations were performed employing the Qlua [37] software suite. S.M. is supported by the U.S. DOE, Office of Science, Office of High Energy Physics under Award Number DE-SC0009913. M.E., J.N. and A.P. are supported by the U.S. DOE, Office of Science, Office of Nuclear Physics through grants numbered DE-FG02-96ER40965, DE-SC-0011090 and DE-SC0023116, respectively. S.S. is supported by the National Science Foundation under CAREER Award PHY-1847893. This work was furthermore supported by the U.S. DOE through the TMD Topical Collaboration.

References

[1] D. Boer, M. Diehl, R. Milner, R. Venugopalan, W. Vogelsang, *et al.*, `arXiv:1108.1713`.

[2] M. Alekseev, *et al.*, COMPASS Collaboration, *Phys. Lett.* **B673** (2009) 127.

[3] A. Airapetian, *et al.*, HERMES Collaboration, *Phys. Rev. Lett.* **103** (2009) 152002.

[4] H. Avakian, *et al.*, CLAS Collaboration, *Phys. Rev. Lett.* **105** (2010) 262002.

[5] S. M. Aybat and T. C. Rogers, *Phys. Rev.* **D 83** (2011) 114042.

[6] J. C. Collins, *Foundations of Perturbative QCD* (Cambridge University Press, 2011).

[7] S. M. Aybat, J. C. Collins, J.-W. Qiu and T. C. Rogers, *Phys. Rev.* **D 85** (2012) 034043.

[8] J. C. Collins and T. C. Rogers, *Phys. Rev.* **D 87** (2013) 034018.

[9] L. Adamczyk, *et al.*, STAR Collaboration, *Phys. Rev. Lett.* **116** (2016) 132301.

[10] M. Aghasyan, *et al.*, COMPASS Collaboration, *Phys. Rev. Lett.* **119** (2017) 112002.

[11] M. Anselmino, M. Boglione, U. D'Alesio, F. Murgia and A. Prokudin, *JHEP* **04** (2017) 046.

[12] B. Musch, P. Hägler, M. Engelhardt, J. W. Negele and A. Schäfer, *Phys. Rev.* **D 85** (2012) 094510.

[13] M. Engelhardt, P. Hägler, B. Musch, J. Negele and A. Schäfer, *Phys. Rev.* **D 93** (2016) 054501.

[14] B. Yoon, M. Engelhardt, R. Gupta, T. Bhattacharya, J. R. Green, B. Musch, J. Negele, A. Pochinsky, A. Schäfer, and S. Syritsyn, *Phys. Rev.* **D 96** (2017) 094508.

[15] M. Engelhardt, *Phys. Rev.* **D 95** (2017) 094505.

[16] M. Engelhardt, J. R. Green, N. Hasan, S. Krieg, S. Meinel, J. Negele, A. Pochinsky and S. Syritsyn, *Phys. Rev.* **D 102** (2020) 074505.

[17] M. Engelhardt, J. R. Green, N. Hasan, T. Izubuchi, C. Kallidonis, S. Krieg, S. Liuti, S. Meinel, J. Negele, A. Pochinsky A. Rajan, G. Silvi and S. Syritsyn, *PoS* **LATTICE2021** (2022) 413.

[18] M. Ebert, I. Stewart and Y. Zhao, *JHEP* **09** (2019) 037.

[19] M. Ebert, S. Schindler, I. Stewart and Y. Zhao, *JHEP* **04** (2022) 178.

[20] X. Ji, Y. Liu and Y.-S. Liu, *Nucl. Phys.* **B955** (2020) 115054.

[21] M. Constantinou, H. Panagopoulos and G. Spanoudes, *Phys. Rev.* **D 99** (2019) 074508.

[22] P. Shanahan, M. Wagman and Y. Zhao, *Phys. Rev.* **D 101** (2020) 074505.

[23] J. Green, K. Jansen and F. Steffens, *Phys. Rev.* **D 101** (2020) 074509.

[24] Y. Ji, J.-H. Zhang, S. Zhao and R. Zhu, *Phys. Rev.* **D 104** (2021) 094510.

[25] T. Blum, P. Boyle, N. Christ, J. Frison, N. Garron, R. Hudspith, T. Izubuchi, T. Janowski, C. Jung, A. Juettner, C. Kelly, R. Kenway, C. Lehner, M. Marinkovic, R. Mawhinney, G. McGlynn, D. Murphy, S. Ohta, A. Portelli, C. Sachrajda and A. Soni, RBC/UKQCD Collaboration, *Phys. Rev.* **D 93** (2016) 074505.

[26] E. Shintani, R. Arthur, T. Blum, T. Izubuchi, C. Jung and C. Lehner, *Phys. Rev.* **D 91** (2015) 114511.

[27] S. Ohta, *PoS* **LATTICE2021** (2022) 529.

[28] N. Hasan, J. R. Green, S. Meinel, M. Engelhardt, S. Krieg, J. Negele, A. Pochinsky and S. Syritsyn, *Phys. Rev.* **D 99** (2019) 114505.

[29] J. He, D. Brantley, C. C. Chang, I. Chernyshev, E. Berkowitz, D. Howarth, C. Körber, A. Meyer, H. Monge-Camacho, E. Rinaldi, C. Bouchard, M. Clark, A. Gambhir, C. Monahan, A. Nicholson, P. Vranas and A. Walker-Loud, *Phys. Rev.* **C 105** (2022) 065203.

[30] R. Jakob, P. Mulders and J. Rodrigues, *Nucl. Phys.* **A626** (1997) 937.

[31] B. Pasquini, S. Cazzaniga and S. Boffi, *Phys. Rev.* **D 78** (2008) 034025.

[32] H. Avakian, A. Efremov, P. Schweitzer and F. Yuan, *Phys. Rev.* **D 81** (2010) 074035.

[33] J. Zhu and B.-Q. Ma, *Phys. Lett.* **B696** (2011) 246.

[34] C. Lorcé, B. Pasquini and M. Vanderhaeghen, *JHEP* **05** (2011) 041.

[35] A. Efremov, P. Schweitzer, O. Teryaev and P. Zavada, *Phys. Rev.* **D 80** (2009) 014021.

[36] Jülich Supercomputing Centre, *JURECA: Modular supercomputer at Jülich Supercomputing Centre*. *Journal of Large-Scale Research Facilities* **4** (2018) A132. http://dx.doi.org/10.17815/jlsrf-4-121-1

[37] A. Pochinsky, *Qlua*. https://usqcd.lns.mit.edu/qlua.